

THE SYSTEM Fe–Os–S AT 1180°, 1100° AND 900°C

SVEN KARUP-MØLLER

Institute of Geology and Geological Engineering, Danish Technical University, DK-2800 Lyngby, Denmark

EMIL MAKOVICKY[§]

Geological Institute, University of Copenhagen, Øster Voldgade 10, DK-1350 Copenhagen K, Denmark

ABSTRACT

Phase relations in the condensed system Fe–Os–S were investigated by means of dry syntheses from the elements at 1180°, 1100° and 900°C. The Fe-rich sulfide melt dissolves only traces of Os. Fe_{1-x}S dissolves up to 0.7 at.% Os at 1180°C; Os solubility decreases to 0.3 at.% at 900°C. The S-rich sulfide melt dissolves up to 0.5 at.% Os at 1180°C. The principal Fe–Os alloys at all temperatures studied are cubic γ (Fe,Os), rhombohedral (Os,Fe) and nearly pure Os. The bulk of Fe–Os alloys coexist with Fe-rich sulfide melt and S-poor Fe_{1-x}S; we provide Nernst partition coefficients for Os. The three-phase association alloy – Fe_{1-x}S – OsS₂ involves alloys with less than 1 at.% Fe. The solubility of Fe in OsS₂ increases with decreasing temperature and increasing fugacity of sulfur, possibly making analyses of erlichmanite for trace quantities of Fe important.

Keywords: system Fe–Os–S, iron–osmium alloys, X-ray diffraction, monosulfide solid-solution, erlichmanite.

SOMMAIRE

Nous avons étudié les relations de phases du système condensé Fe–Os–S au moyen de synthèses à sec à partir des éléments à 1180°, 1100° et 900°C. Le liquide sulfuré riche en fer ne peut dissoudre que des traces d'osmium. La phase Fe_{1-x}S dissout jusqu'à 0.7% d'osmium (proportion atomique) à 1180°C; la solubilité diminue jusqu'à 0.3% à 900°C. Le liquide sulfuré riche en soufre dissout jusqu'à 0.5% d'Os à 1180°C. Les alliages principaux de Fe–Os aux trois températures choisies sont la phase γ (Fe,Os), cubique, la phase rhomboédrique (Os,Fe), et l'osmium presque pur. Dans la plupart des cas, les alliages Fe–Os coexistent avec un liquide sulfuré riche en Fe et la phase Fe_{1-x}S, pauvre en soufre. Nous fournissons des coefficients de partage de Nernst pour l'osmium. L'association à trois phases alliage – Fe_{1-x}S – OsS₂ implique un alliage contenant moins de 1% de Fe (proportion atomique). La solubilité du fer dans OsS₂ augmente à mesure que diminue la température et qu'augmente la fugacité en soufre, de sorte qu'il pourrait s'avérer important d'analyser l'erlichmanite pour évaluer les quantités de fer qu'elle contient.

(Traduit par la Rédaction)

Mots-clés: système Fe–Os–S, alliage fer–osmium, diffraction X, solution solide monosulfurée, erlichmanite.

INTRODUCTION

In connection with the growing geochemical importance of the Re–Os pair, we have investigated the systems Fe–Re–S and Fe–Os–S at magmatic temperatures. Our results on the system Fe–Re–S have been published (Karup-Møller & Makovicky 1999). Here we report on the system Fe–Os–S at 1180°, 1100° and 900°C. At these temperatures, the condensed dry Fe–Os–S system contains three Fe–Os alloys, the molten iron sulfide, Fe_{1-x}S solid solution and OsS₂, the only osmium sulfide found.

Previous investigations of the partial systems involved were performed by Fishman *et al.* (1992), who determined the Os–OsS₂ eutectic, and Swartendruher (1983), who provided a calculated phase-diagram for the system Fe–Os between 400° and 3000°C.

EXPERIMENTAL

Seventy-one 100-mg charges were weighed out from pure elements (Os powder, freshly filed specpure Fe rods from Johnson Matthey Ltd. with 15 ppm metallic impurities, and sulfur from Fluka, >99.999%). The

[§] E-mail address: emilm@geo.geol.ku.dk

mixtures were sealed in evacuated silica glass tubes, preheated at 300°C, and annealed in vertical furnaces at the desired temperatures for periods of up to 15 days. Regrinding and homogenization were applied to the charges, together with subsequent pelletization, resealing and annealing at the same temperatures for up to 30 days.

The annealed products were quenched by straight drop in cold water, prepared as polished sections, and studied in reflected light and by means of electron-microprobe analyses. A JEOL Superprobe 733 was used in wavelength-dispersion mode. The on-line correction program was supplied by JEOL. Wavelengths and standards employed were $OsL\alpha$ (standard was pure Os metal), $FeK\alpha$ and $SK\alpha$ (synthetic FeS as standard for both elements); the excitation voltage was 20 kV, sample current, 30 nA, and counting times, up to 20 s. At least ten measurements were taken on each phase present and subsequently averaged. The detection limits for alloys were 0.04 wt%, *i.e.*, ~0.02 at.% for Os and ~0.01 wt% (0.03 at.%) for Fe, on the basis of results obtained from pure phases synthesized without minor elements. Ten to twenty measurements were taken on solidified melts using a sweeping beam at magnifications between 3600 and 10000 \times depending on the grain size of the crystals in the quenched liquid. The principal results are given in Tables 1a, 1b and 1c.

The low-S portions of the system Fe–Os–S are fairly intractable, owing to poor reactivity of Fe–Os alloys, especially in the Os-rich part of the system. This fact, together with the very small size of alloy grains, generally amalgamated into a loose three-dimensional aggregate, led to a significant spread of analytical results. A similar situation also causes problems when analyzing the synthesized OsS_2 phase. Difficulties encountered in quenching of the mush composed of melt and very small crystals of alloy, and in finding sufficiently large homogeneous areas in it, also had an adverse influence on the quality of the estimated values of the Fe:S ratio obtained for the melt.

PHASE RELATIONS AT 1180°C

At this temperature, the system Fe–Os–S contains three alloys, two melts and two sulfides (Fig. 1). Detailed mapping of the phase relationships and electron-microprobe analyses have revealed the presence of two alloys with extensive solid-solution fields: (a) isotropic γ (Fe,Os) reaching to 21.5 at.% Os, and (b) (Os,Fe) from 27.3 at.% Os toward high Os contents. It displays an increasing degree of anisotropy in polished sections with increasing Os content. In spite of a detailed examination of the (Os,Fe) alloy with high Os contents, no compositional gap could be ascertained in the latter from the electron-microprobe data alone.

The entire compositional range of the γ alloy and most of the range of the (Os,Fe) alloy coexist with S-poor sulfide melt. At its sulfur-poorest compositions,

this melt is Os-free (0–0.02 at.%). The gap between the γ phase and rhombohedral (Os,Fe) coexists with the melt with ~56.7 at.% Fe. At the melt compositions richest in S, the solubility of Os increases to 0.06–0.10 at.% Os (at 50 at.% S). These coexist with the (Os,Fe)

TABLE 1a. ELECTRON-MICROPROBE-BASED COMPOSITIONS OF SELECTED PHASES IN THE SYSTEM Os–Fe–S at 1180°C

Charge	Phase	N	Os	Fe	S	Sum
120s1	Alloy	18	20.99(60)	80.63(99)	0.04(2)	101.66
120s1	Liquid	27	0.04(3)	70.11(100)	30.67(79)	100.82
120s2	Alloy	19	40.32(58)	61.20(89)	0.03(2)	101.55
120s2	Liquid	48	0.05(5)	70.34(154)	30.39(124)	100.78
120s3	Alloy	15	61.28(100)	39.98(85)	0.05(2)	101.31
120s3	Liquid	37	0.07(6)	68.76(248)	32.11(216)	100.94
120s4	Alloy	22	73.37(55)	27.73(36)	0.05(2)	101.15
120s4	Liquid	14	0.04(3)	70.03(440)	30.98(405)	101.05
120s5	Alloy	12	82.39(57)	19.13(60)	0.09(4)	101.62
120s5	Liquid	20	0.03(2)	66.42(79)	32.88(81)	99.33
120s6	Alloy	12	92.65(45)	8.95(28)	0.09(5)	101.70
120s6	Liquid	12	0.08(3)	66.55(94)	32.87(97)	99.50
120s7	Alloy	7	99.96(23)	0.97(7)	0.07(3)	101.00
120s7	Liquid	20	0.12(6)	64.03(37)	36.14(38)	100.28
120s8	Alloy	6	101.51(47)	0.18(4)	0.04(2)	101.74
120s8	<i>mss</i>	24	1.62(15)	60.35(37)	38.51(30)	100.47
120s11	Alloy	2	102.78(0)	0.05(0)	0.03(0)	102.86
120s11	OsS_2	18	76.03(62)	0.14(3)	24.22(29)	100.40
120s11	<i>mss</i>	19	2.69(32)	59.14(51)	38.44(71)	100.27
120s14	Alloy	9	102.17(90)	0.03(2)	0.06(3)	102.26
120s14	OsS_2	16	75.02(55)	0.21(3)	24.38(29)	99.61
120s14	<i>mss</i>	19	1.98(9)	60.31(20)	38.35(33)	100.64
120s15	Alloy-1	2	99.49(40)	0.01(0)	0.02(2)	99.53
120s15	Alloy-1	2	62.46(23)	34.78(27)	0.03(4)	97.26
120s15	OsS_2	17	75.90(27)	0.10(3)	24.34(37)	100.34
120s15	<i>mss</i>	11	2.48(22)	59.89(31)	38.63(36)	101.00
120s16	OsS_2	15	74.16(24)	0.56(12)	24.79(17)	99.51
120s16	Liquid	22	0.98(50)	58.81(50)	40.58(58)	100.36
120s17	OsS_2	17	74.42(79)	0.74(24)	24.64(39)	99.79
120s17	Liquid	20	0.87(27)	59.34(90)	39.96(78)	100.17
120s18	OsS_2	13	74.61(103)	0.72(15)	24.46(32)	99.79
120s18	Liquid	19	0.72(25)	58.77(208)	39.41(213)	98.90
120s38	Liquid	3	0.51(12)	63.51(70)	35.51(104)	99.52
120s38	Alloy	7	94.37(43)	6.26(32)	0.07(6)	100.70
120s39	Liquid	3	0.39(23)	62.94(27)	35.94(47)	99.27
120s39	Alloy	8	97.64(254)	3.09(217)	0.02(1)	100.75
120s40	Liquid	3	0.27(8)	63.36(20)	36.29(37)	99.91
120s40	Alloy	5	98.03(100)	3.34(71)	0.03(3)	101.41
120s41	Alloy-1	22	47.81(70)	52.62(75)	0.07(7)	100.50
120s41	Alloy-2	2	55.89(0)	43.70(0)	0.01(0)	99.60
120s42	Alloy	24	67.81(67)	32.48(63)	0.04(3)	100.33

N: number of analyses made. Compositions expressed in wt.%, with standard deviations given in brackets. *mss*: monosulfide solid-solution.

alloy with microprobe-established compositions of ≥ 81 at.% Os.

At about 98.5 at.% Os in the alloy, a three-phase association of melt (~ 50 at.% Fe with ~ 0.1 at.% Os) – Fe_{1-x}S (~ 47.2 at.% Fe and 0.4 at.% Os) – alloy occurs. The solubility of Os in Fe_{1-x}S increases toward 0.7 at.% Os at ~ 46.6 at.% Fe, in the three-phase association Fe_{1-x}S – alloy (99.5–99.7 at.% Os) – OsS_2 (0.2 at.% Fe).

The S-rich sulfide melt had to be positioned on the Fe–S join according to the findings of Kubaschewski

(1982). Its Os content varies between 0.2 and 0.5 at.% Os, with Os contents decreasing with the increasing original, pre-quench S contents of the melt. The solubility of Fe in the associated OsS_2 is a sensitive function of S content: for the association with Fe_{1-x}S and sulfide melt, it is about 0.2 at.% Fe (~ 34.4 at.% Os), and it gradually increases to 1.1 at.% Fe (or higher) for the most S-rich associations OsS_2 (~ 33.3 at.% Os) – melt \pm sulfur.

TABLE 1b. ELECTRON-MICROPROBE-BASED COMPOSITIONS OF SELECTED PHASES IN THE SYSTEM Os–Fe–S at 1100°C

Charge	Phase	N	Os	Fe	S	Sum
11Os1	Alloy	7	36.23(61)	66.54(52)	0.10(10)	102.88
11Os1	Liquid	14	0.04(3)	71.06(43)	31.87(40)	102.96
11Os2	Alloy	5	55.96(20)	46.35(59)	0.07(4)	102.38
11Os2	Liquid	14	0.04(4)	70.53(111)	32.67(102)	103.24
11Os3	Alloy	4	64.19(29)	37.42(20)	0.07(1)	101.68
11Os3	Liquid	19	0.66(197)	68.14(331)	33.40(255)	102.20
11Os4	Alloy	6	72.61(93)	29.63(74)	0.07(3)	102.32
11Os4	Liquid	15	0.06(4)	69.11(98)	33.70(101)	102.87
11Os5	Alloy	5	79.57(57)	22.41(32)	0.12(2)	102.10
11Os5	Liquid	19	0.04(3)	68.72(87)	33.81(89)	102.57
11Os6	Alloy	7	87.35(77)	14.69(73)	0.10(4)	102.14
11Os6	Liquid	14	0.09(6)	67.72(59)	34.81(45)	102.62
11Os7	Alloy-1	6	92.55(50)	9.31(32)	0.08(5)	101.95
11Os7	Alloy-2	3	100.53(58)	0.49(7)	0.08(5)	101.11
11Os7	<i>mss</i>	36	0.16(15)	64.95(54)	37.31(23)	102.42
11Os8	Alloy	5	100.99(50)	0.26(9)	0.05(2)	101.30
11Os8	<i>mss</i>	16	0.55(23)	62.85(27)	37.71(35)	101.11
11Os9	Alloy	5	100.48(80)	0.27(17)	0.06(3)	100.81
11Os9	OsS_2 -1	2	74.85(136)	1.21(17)	23.99(19)	100.04
11Os9	OsS_2 -2	5	72.40(163)	0.69(8)	25.17(56)	98.26
11Os9	<i>mss</i>	5	1.90(20)	59.84(51)	39.40(36)	101.14
11Os11	Alloy	3	100.60(50)	0.03(1)	0.10(3)	100.73
11Os11	OsS_2	6	74.96(26)	0.14(3)	24.83(14)	99.92
11Os11	<i>mss</i>	6	1.99(17)	61.38(22)	39.53(33)	102.90
11Os12	Alloy	2	99.18(0)	0.04(0)	0.02(0)	99.24
11Os12	OsS_2	5	74.31(31)	0.12(4)	24.83(24)	99.26
11Os12	<i>mss</i>	10	1.73(28)	58.25(46)	38.04(35)	98.02
11Os13	Alloy	3	100.44(43)	0.13(4)	0.08(3)	100.65
11Os13	OsS_2	4	73.88(22)	0.30(8)	24.79(9)	98.97
11Os13	<i>mss</i>	11	1.45(11)	59.09(48)	38.08(29)	98.63
11Os14	OsS_2	6	73.77(31)	1.09(34)	24.88(24)	99.74
11Os14	<i>mss</i>	10	1.08(10)	59.02(37)	38.79(23)	98.89
11Os15	OsS_2	3	73.30(15)	0.69(13)	25.08(13)	99.06
11Os15	<i>mss</i>	11	1.32(13)	59.30(43)	38.40(20)	99.03
11Os16	OsS_2	4	73.22(62)	1.33(8)	24.97(33)	99.52
11Os16	<i>mss</i>	12	1.12(38)	59.24(55)	38.73(42)	99.09
11Os41	Alloy-1	18	46.68(23)	54.07(24)	0.06(5)	100.81
11Os41	Alloy-2	5	56.47(60)	44.16(21)	0.01(0)	100.64

N: number of analyses made. Compositions expressed in wt.%, with standard deviations given in brackets. *mss*: monosulfide solid-solution.

TABLE 1c. ELECTRON-MICROPROBE-BASED COMPOSITIONS OF SELECTED PHASES IN THE SYSTEM Os–Fe–S at 900°C

Charge	Phase	N	Os	Fe	S	Sum
9Os1	Alloy	32	62.43(166)	38.09(151)	0.06(4)	100.58
9Os1	<i>mss</i>	9	0.09(4)	63.78(23)	36.04(30)	99.91
9Os2	Alloy-1	10	94.09(541)	6.33(479)	0.08(6)	100.49
9Os2	Alloy-2	6	80.82(191)	18.25(51)	0.07(6)	99.14
9Os2	<i>mss</i>	9	0.48(40)	63.34(41)	36.22(28)	100.04
9Os3	Alloy-1	10	100.12(82)	0.20(8)	0.08(6)	100.40
9Os3	Alloy-2	4	74.06(390)	16.26(141)	0.05(3)	90.36
9Os3	<i>mss</i>	10	0.31(10)	62.71(21)	36.56(27)	99.58
9Os4	Alloy	3	100.90(44)	0.02(0)	0.03(2)	100.95
9Os4	<i>mss</i>	10	1.26(27)	60.20(34)	37.79(27)	99.25
9Os5	Alloy	4	101.28(102)	0.03(2)	0.07(5)	101.37
9Os5	<i>mss</i>	13	1.16(27)	60.04(33)	38.08(25)	99.28
9Os7	Alloy	4	101.40(45)	0.22(16)	0.12(1)	101.75
9Os7	OsS_2	6	75.26(51)	0.28(5)	21.30(57)	96.85
9Os7	<i>mss</i>	10	0.58(16)	60.46(19)	37.89(12)	98.93
9Os8	OsS_2	6	74.26(68)	0.44(16)	24.72(38)	99.41
9Os8	<i>mss</i>	10	0.70(12)	59.72(18)	38.76(19)	99.18
9Os9	OsS_2	6	69.24(146)	2.46(72)	26.45(104)	98.14
9Os9	<i>mss</i>	14	0.25(27)	59.08(45)	39.78(53)	99.10
9Os10	Alloy	6	18.67(95)	78.91(119)	0.04(5)	97.62
9Os10	<i>mss</i>	9	0.07(3)	62.84(34)	36.17(16)	99.09
9Os11	Alloy	8	35.85(165)	62.64(127)	0.04(3)	98.53
9Os11	<i>mss</i>	8	0.03(2)	62.87(55)	36.21(23)	99.11
9Os12	Alloy	10	53.61(69)	44.94(70)	0.05(4)	98.60
9Os12	<i>mss</i>	9	0.05(3)	62.74(40)	36.23(19)	99.01
9Os13	Alloy	12	69.55(100)	29.08(83)	0.04(3)	98.68
9Os13	<i>mss</i>	7	0.09(7)	62.48(40)	36.26(35)	98.83
9Os14	Alloy	14	76.36(89)	23.32(184)	0.03(2)	99.71
9Os14	<i>mss</i>	11	0.23(7)	62.44(37)	36.32(50)	98.99
9Os15	Alloy	12	77.89(532)	14.63(143)	0.16(13)	92.68
9Os15	<i>mss</i>	9	0.38(11)	62.17(41)	36.36(42)	98.90
9Os16	Alloy	14	87.93(700)	5.28(345)	0.08(5)	93.28
9Os16	<i>mss</i>	9	0.54(18)	61.83(35)	36.58(26)	98.95
9Os17	Alloy	18	89.72(253)	3.68(101)	0.07(5)	93.48
9Os17	Alloy	3	97.54(157)	0.96(53)	0.02(1)	98.53
9Os17	<i>mss</i>	7	0.38(7)	62.64(35)	36.65(18)	99.66
9Os18	Alloy	10	98.02(336)	0.15(10)	0.04(3)	98.21
9Os18	<i>mss</i>	11	0.48(10)	60.97(44)	38.00(29)	99.46
9Os19	<i>mss</i>	9	0.23(6)	58.60(29)	40.77(30)	99.60

N: number of analyses made. Compositions expressed in wt.%, with standard deviations given in brackets. *mss*: monosulfide solid-solution.

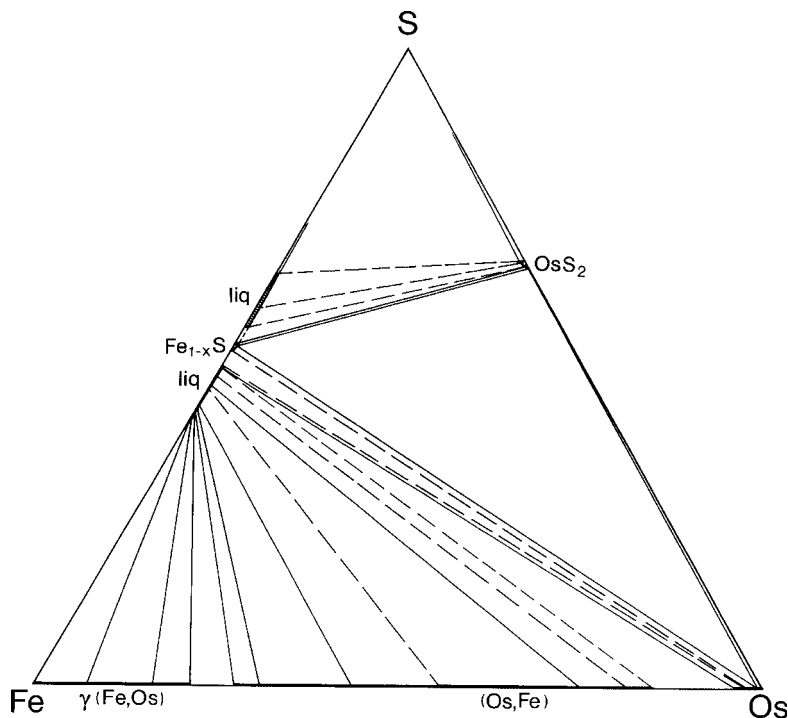


FIG. 1. Phase diagram for the system Fe–Os–S at 1180°C.

PHASE RELATIONS AT 1100°C

At this temperature, the system contains the same number of phases as at 1180°C (Fig. 2). The cubic γ (Fe,Os) phase coexists with more Fe-rich Os-free portions of the Fe-rich (Fe,S) liquid, typified by a pair: $\text{Fe}_{86.2}\text{Os}_{13.8} - \text{Fe}_{56.1}\text{Os}_{0.01}\text{S}_{43.9}$.

The gap between the alloys is defined by a three-phase association γ (Fe,Os) (20.2 at.% Os) – rhombohedral (Os,Fe) (26.1 at.% Os) – liquid (~44.4 at.% S, 0.01 at.% Os, *i.e.*, Os-free). The two-phase field (Fe, S) melt – rhombohedral alloy is typified by joins: $\text{Fe}_{54.3}\text{Os}_{-0.01}\text{S}_{45.7} - \text{Fe}_{66.5}\text{Os}_{33.5}$, $\text{Fe}_{54.1}\text{Os}_{0.01}\text{S}_{45.9} - \text{Fe}_{58.3}\text{Os}_{41.7}$, $\text{Fe}_{53.9}\text{Os}_{0.01}\text{S}_{46.1} - \text{Fe}_{49.6}\text{Os}_{50.4}$, $\text{Fe}_{52.8}\text{Os}_{0.02}\text{S}_{47.2} - \text{Fe}_{36.5}\text{Os}_{63.5}$, $\text{Fe}_{53.0}\text{Os}_{0.01}\text{S}_{47.0} - \text{Fe}_{30.0}\text{Os}_{70.0}$.

The three-phase association (Os,Fe) alloy – (Fe,S) melt – Fe_{1-x}S , with 71–72 at.% Os in the alloy, and 0.01 at.% Os in the associated phases, is followed by a two-phase field Fe_{1-x}S – alloy, typified by the pairs of microprobe-established compositions: troilite (0.02 at.% Os) – $\text{Fe}_{25.6}\text{Os}_{74.4}$ and $\text{Fe}_{48.9}\text{Os}_{0.1}\text{S}_{51.0} - \text{Fe}_{0.8}\text{Os}_{99.2}$. The exact relationship of these pairs was resolved only by means of X-ray powder diffraction.

In the three-phase association Fe_{1-x}S – alloy – OsS_2 , the phases have an estimated composition $\text{Fe}_{46.5}\text{Os}_{0.5}\text{S}_{53.0}$, $\text{Fe}_{0.3}\text{Os}_{99.7}$ (uncertainty ± 0.2 at.%) and OsS_2 (≤ 0.4 at.% Fe). In the ensuing two-phase association $\text{Fe}_{1-x}\text{S} - \text{OsS}_2$,

mss with about 53.2 at.% S has 0.3 at.% Os, and the Fe content in OsS_2 attains 1.9 at.%. In the charge that appears texturally to consist of *mss* and S-rich melt, *mss* with at least 53.3 at.% S contains 0.25 at.% Os, whereas there is 2.0 at.% Fe in OsS_2 . The system is completed by a three-phase assemblage melt [0.14 at.% Os; the initial S content of ~64.6 at.% (Massalski *et al.* 1986) was reduced by a boil-off of sulfur on quenching to 54.4 at.%] – OsS_2 (at least 2.9 at.% Fe) – S.

PHASE RELATIONS AT 900°C

At this temperature, the system Fe–Os–S contains two alloys with broad solid-solution fields, Os and two sulfides (Fig. 3).

The cubic γ (Fe,Os) solid solution and the rhombohedral (Os,Fe) solid solution are separated by a gap constrained by two well-defined two-phase assemblages, with 14.4 at.% Os and 25.9 at.% Os in the alloy, respectively, both associated with Fe_{1-x}S that has 50.1 at.% S and is Os-free (≤ 0.01 at.% Os measured). The three-phase assemblage γ (Fe,Os) – rhombohedral (Os,Fe) – Fe_{1-x}S can be further constrained to 17.2 and 24.2 at.% of the dominant element in the two respective alloys, both values being based on several microprobe-based measurements. On the basis of the calculated phase-diagram (Swartendruher 1983) the α – γ association is

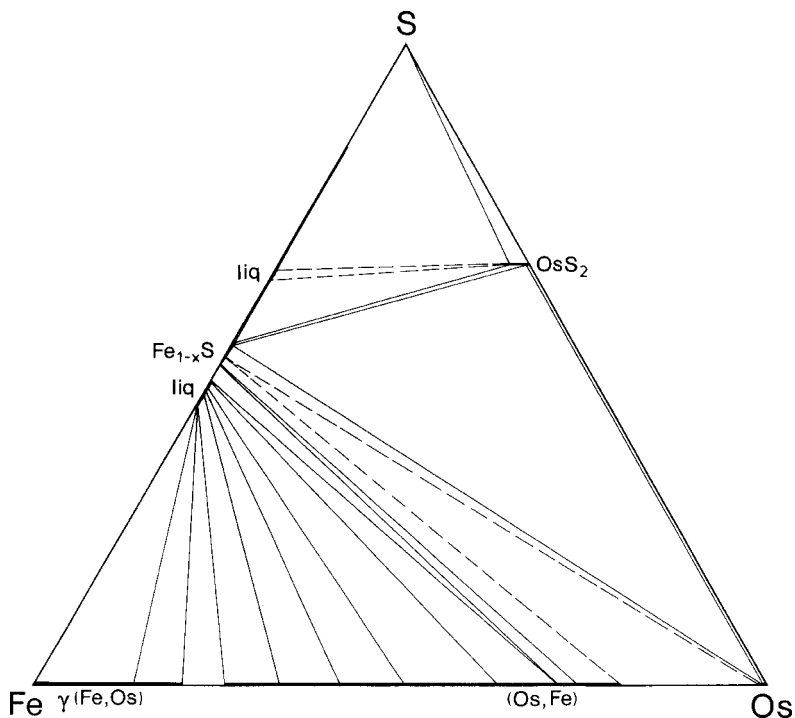


FIG. 2. Phase diagram for the system Fe–Os–S at 1100°C.

expected to be confined to the first atomic percent of the Fe–Os solid solution; it was not investigated because of reactivity problems.

In the Os-rich region, the low reactivity of Os leads to broad or very broad compositional ranges and low-accuracy estimates of composition for the alloys involved in two-phase assemblages alloy – Fe_{1-x}S . Therefore, no compositional gaps could be established with certainty in the alloys by microprobe measurements alone.

Typical two-phase assemblages Fe_{1-x}S – rhombohedral alloy are (in at.%): $\text{Fe}_{49.9}\text{Os}_{0.01}\text{S}_{50.1}$ – $\text{Fe}_{74.1}\text{Os}_{25.9}$, $\text{Fe}_{49.7}\text{Os}_{0.02}\text{S}_{50.3}$ – $\text{Fe}_{58.8}\text{Os}_{41.2}$, $\text{Fe}_{49.6}\text{Os}_{0.06}\text{S}_{50.3}$ – $\text{Fe}_{42}\text{Os}_{58}$, and $\text{Fe}_{49.5}\text{Os}_{0.09}\text{S}_{50.4}$ – $\text{Fe}_{12.6}\text{Os}_{87.4}$. The last, broadly scattered alloy composition in this list falls into the two-phase region defined by X-ray powder diffraction further below.

The three-phase association Fe_{1-x}S – (Os,Fe) – OsS_2 is characterized by the compositions $\text{Fe}_{47.4}\text{Os}_{0.3}\text{S}_{52.3}$ – $\text{Os}_{99.8}\text{Fe}_{0.2}$ – OsS_2 (0.2 at.% Fe). Iron monosulfide with still higher contents of S coexists with OsS_2 until the three-phase association Fe_{1-x}S (54.8 at.% S, 0.05 at.% Os) – OsS_2 (5.7 at.% Fe, 66.2 at.% S) – S is reached. Typical binary pairs are: $\text{Fe}_{46.8}\text{Os}_{0.2}\text{S}_{53.0}$ – OsS_2 (0.7 at.% Fe) and $\text{Fe}_{45.9}\text{Os}_{0.1}\text{S}_{54.0}$ – OsS_2 (4.2 at.% Fe). Decreasing content of Os with increasing S contents in

Fe_{1-x}S is paralleled by a strongly increasing Fe content in OsS_2 .

X-RAY POWDER-DIFFRACTION DATA

An attempt was made to investigate the potential gaps in the (Fe,Os) alloys by means of X-ray powder diffraction, starting with the samples synthesized at 1180°C. A Guinier–Hägg camera was employed, using $\text{CuK}\alpha_1$ radiation and quartz as an internal standard. The unit-cell parameters of the rhombohedral (Os,Fe) solid solution were refined by a least-squares procedure from a set of eight reflections, and in the Fe-rich cases, five reflections. In the most Fe-rich charges, only three usable reflections could be found.

The lines used were 100, 002, 101, 102, 110, 103, 112 and 201 of the hexagonal cell; the first three lines persist longest with progressively Fe-enriched compositions. On the one hand, the unchanging 2.025 Å, 110 line of α -Fe persists at 1180°C in traces even for the charge with the $\text{Os}_{.75}\text{Fe}_{.25}$ alloy (charge No. 12–6; all alloy compositions given are averaged microprobe-based data), disappearing only in the charge $\text{Os}_{.98}\text{Fe}_{.2}$ (no. 12–7). On the other hand, two phantom lines of the hexagonal phase are still present in the charge no. 12–2 ($\text{Fe}_{.84.4}\text{Os}_{.15.6}$), whereas they are absent in

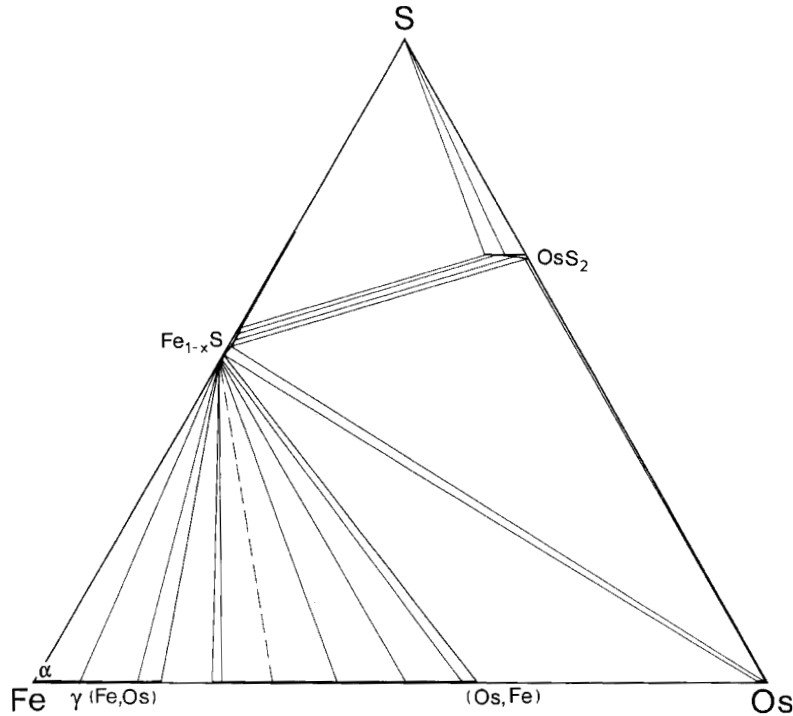


FIG. 3. Phase diagram for the system Fe-Os-S at 900°C.

no. 12-1. Troilite lines with d values unchanged are present in all patterns.

There is a linear change in the a and c parameters of the rhombohedral phase with the $Os/(Os + Fe)$ value. As seen in Figure 4, the linear trend for the c value extends over the range $Os_{-15.6} - Os_{-75}$ at 1180°C. The trend is modified above Os_{75} , with a somewhat slower increase in cell dimensions with the increasing percentage of Os in the alloy. Results are tabulated in Table 2.

Practically the entire spectrum of alloys at 1180°C coexists with the Fe-rich sulfide melt; it yields, on quenching, α -Fe and troilite, detected in the X-ray diffractograms. As mentioned above, the decrease of a and c parameters in the quenched samples can still be traced at about 15 at.% Os in the alloy, *i.e.*, beyond the field of the rhombohedral phase and into the field of γ (Fe,Os) at 1180°C. In this case, we must be dealing with the rhombohedral phase exsolved from the γ phase on quenching.

In order to investigate the potential gap between nearly pure Os and the rhombohedral (Os,Fe) alloy at lower temperatures, X-ray powder-diffraction analysis was extended to selected charges from 900° and 1100°C.

At 1100°C, charges with alloys $Fe_{-34.2}Os_{-65.8} - Fe_{-24.1}Os_{-75.9}$, and with only traces of unreacted osmium

in polished section, show only one alloy phase in the Guinier powder diagrams. Charges with ~83 at.% Os or more show two alloy phases (Table 2). One phase has

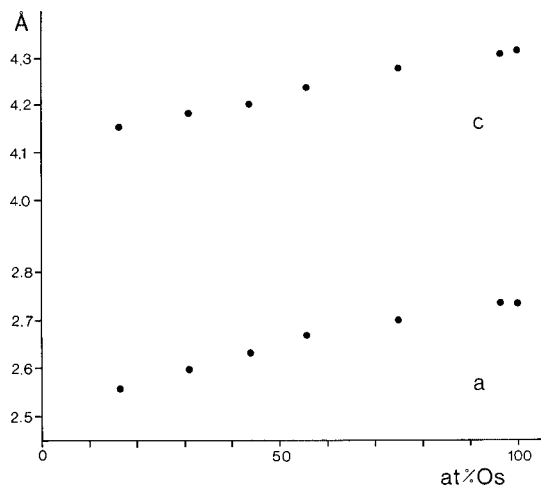


FIG. 4. Refined unit-cell parameters a and c of the rhombohedral (Os,Fe) alloy. Horizontal axis: microprobe-based average compositions. Error bars are commensurate with the dot size.

TABLE 2. REFINED UNIT-CELL DIMENSIONS FOR RHOMBOHEDRAL (Os,Fe) ALLOY COMPOSITIONS QUENCHED FROM 1180°, 1100° AND 900°C

Sample	12-2	12-3**	12-4	12-5	
at.% Os	16.2	31	43.6	55.6	
<i>a</i> (Å)	~2.561	2.601(6)	2.632(2)	2.660(1)	
<i>c</i> (Å)	~4.154	4.180(11)	4.200(6)	4.238(2)	
Sample	12-6	12-7***	std		
at.% Os	74.9	96.4	100		
<i>a</i> (Å)	2.701(1)	2.733(1)	2.734(0)		
<i>c</i> (Å)	4.280(3)	4.312(2)	4.318(1)		
Sample	11-50	11-38	11-40	11-22	11-23
at.% Os	(98.8)	(98.6)	98.8	~98	~99
	65.8	75.9	82.8	89.2	93.1
<i>a</i> ₁ (Å)	-	-	2.734(1)	2.734(1)	2.734(1)
<i>c</i> ₁ (Å)	-	-	4.314(2)	4.320(2)	4.317(2)
<i>a</i> ₂ (Å)	2.677(1)	2.700(1)	2.711(1)	2.702(1)	2.713(0)
<i>c</i> ₂ (Å)	4.260(3)	4.279(2)	4.288(3)	4.281(2)	4.292(1)
I ₁ /I ₂ (101)	0:10	0:10	7:8	9:4	7:1
Sample	9-15	9-16	9-17	9-18	
at.% Os	~98	98.1	ave. 88	99.2	
	60.5	67.3			
<i>a</i> ₁ (Å)	2.734(0)	2.735(1)	2.734(0)	2.734(0)	
<i>c</i> ₁ (Å)	4.319(1)	4.320(1)	4.320(1)	4.319(1)	
<i>a</i> ₂ (Å)	2.665(1)	2.672(1)	2.685(1)	-	
<i>c</i> ₂ (Å)	4.243(2)	4.255(2)	4.264(2)	-	
I ₁ /I ₂ (101)	10:7	10:3	10:2	10:0	

The relative intensities of the (101) peak [I₁/I₂(101)] was estimated visually. Values in brackets indicate one standard deviation in terms of the last digit. ** *d*₀₀₂ excluded because of overlap with the standard used. *** *d*₁₁₀ excluded because of similar overlap. *d*₂₀₀ was not used because of overlaps with the standard in all charges.

practically constant unit-cell parameters, close to those of pure Os; the proportion of this phase increases with the change in microprobe-based composition from 83 to 93 at.% Os. A second phase has a smaller unit-cell, for which the averaged *c*-axis data correspond to about Os₈₀, using the trend established at 1180°C. If the change in the trend on the *a* axis, found for the charge 12–6 at 1180°C and ~75 at.% Os, is accepted, then the *a*-axis data from 1100°C also suggest an Os_{~80} composition for the latter phase.

At 900°C, even the charge with the lowest Os contents in the alloy, Fe_{39.5}Os_{60.5}, associated with some Os_{~98} grains, displays two hexagonal alloy phases. Again, one phase yields constant *a* and *c* values corresponding to pure Os throughout the composition range, whereas the other has lower *a* and *c* values but indicates a moderate trend toward slightly higher *a* and *c* values as the average Os contents in the alloy increases from 60.5 to 88 at.% (Table 2). As in all other cases, the lines belonging to nearly pure osmium are much sharper than the lines attributed to the alloy phase.

A number of factors influence the final choice from this set of data. These are related both to the synthesis

experiments (probability of equilibration as a function of volume ratios, epitaxy of minor phase on the major one) and to diffraction experiments (Guinier line profile, refinement quality). Critically evaluating these factors, we adopted the results from those charges where both alloy phases are in approximately equal amounts. The final results are identical with the above-quoted ones for 1100°C, whereas for 900°C, they indicate the boundary value of Os_{~59}, in good agreement with the last well-defined clusters of microprobe-based compositions of alloy (Fe_{42–39.5}Os_{58–60.5}).

In conclusion, the combined X-ray powder diffraction and electron-microprobe data indicate a miscibility gap between rhombohedral (Os,Fe) and nearly pure Os. At 900°C, this gap is at Os_{~59}–Os_{~99}, at 1100°C it is Os_{~80}–Os_{~99}, and at 1180°C it is Os_{>80}–Os_{~96.5}. The miscibility gap is only poorly recognizable from microprobe data alone, presumably because of fine intergrowths and the exceedingly small size of alloy particles. We consider this gap to be a primary, high-temperature feature and not a secondary, exsolution-induced phenomenon. If the latter case were true, we could expect that the extent of exsolution would be the same for the charges quenched from all three temperatures examined or it would even be greater for those quenched from higher temperatures.

IMPLICATIONS AND CONCLUSIONS

Low-sulfur region

The solubility limits of γ (Fe,Os) on the Os-rich side established experimentally by us for the interval 1180° – 900°C agree very well with the values calculated by Swartendruher (1983). Those for the rhombohedral (Os,Fe) alloy show a solubility of Fe of at least 6 at.% higher than predicted by Swartendruher. Moreover, the unit-cell parameters obtained for this phase in the Fe-rich run [which was single-phase γ (Fe,Os) at 1200°C and underwent exsolution] indicate that its composition limits extend to ~15 at.% Os (or below) at temperatures that can be extrapolated to approximately 500°C. This situation again contradicts Swartendruher's results, but agrees with the findings of Pearson & Williams (1979), who obtained the rhombohedral (Fe,Os) alloy with 15 and 30 at.% Os by quenching from 1400°C. In separate experiments at 800°C, we found the miscibility gap between the two alloys to lie between 16.6 at.% Os and 25.3 at.% Os, associated with troilite Fe_{49.9}Os_{0.02}S_{50.1}.

Nernst partition coefficients for the pairs alloy – Fe sulfide melt or Fe_{1–x}S are given in Table 3. As in the case of rhenium (Karup-Møller & Makovicky 1999), the coefficients show a marked skew in favor of alloys, especially at low sulfur fugacities. In these charges, <0.02 at.% Os in the melt or *ms* is the analytical threshold, and for many charges the actual Os content is below this value. Therefore the true Nernst partition coefficients for the majority of these charges are

probably smaller than the values given in Table 3. Above ~50 at.% Os in the alloy, the contents of Os in the melt or *mss* and the partition coefficients start to increase. There is also a marked increase in partition coefficients in that area of the system with temperature. If we extrapolate the rising trend of the Nernst partition coefficients backward to low concentrations of osmium, these coefficients should lie in the $n \times 10^{-5}$ range for the low-Os alloy. Thus, at low S fugacities and Os contents, osmium will partition heavily into iron and its alloys.

The bulk of natural osmium alloys (mostly osmium to irridian osmium) from PGE placers contain as a rule below 1 wt% Fe, and those richest in Os contain, with rare exceptions, well below 0.3 wt% Fe or even no detectable iron (Cabri *et al.* 1996). A similar trend, with somewhat higher Fe contents, was observed by Augé & Legendre (1992) for Pt–Fe nuggets from Madagascar. All these occurrences are associated with isoferroplatinum – γ (Pt,Fe) alloys as the principal phases and are interpreted either as cases of exsolution from these or as primary intergrowths. The Os alloys compositionally correspond to our alloy – $\text{Fe}_{1-x}\text{S} - \text{OsS}_2$ association or, in some cases, perhaps to the alloy – Fe_{1-x}S association immediately adjacent to the latter, indicating low Fe activity in isoferroplatinum or in γ (Pt,Fe). The possible influence of the Fe–Os miscibility gap on the exsolved compositions at low temperatures cannot be estimated because of the lack of experimental data.

High-sulfur region

OsS_2 (erlichmanite) displays a remarkable extent of Fe-for-Os substitution, which increases with decreasing temperature and shows a strong dependence on sulfur fugacity. The latter feature could potentially be used to find high-S regimes among the PGM associations. The compilations of compositions in Cabri (1981) and Cabri *et al.* (1996) omit Fe from the list, the rationale being their common association with Pt–Fe alloys and other Fe-rich phases that interfere with the iron determination. Erlichmanite analyzed by Bowles *et al.* (1983), Johan *et al.* (1989) and Augé & Legendre (1992) has Fe contents below, or corresponding to, those in the three-phase association alloy – $\text{Fe}_{1-x}\text{S} - \text{OsS}_2$. Erlichmanite with high Fe-contents could occur as a sublimate in volcanic exhalations characterized by a high fugacity of sulfur.

ACKNOWLEDGEMENTS

This paper is dedicated to our friend and senior colleague, Dr. Louis J. Cabri. We are grateful to our colleagues, Dr. Milota Makovicky and Associate Professor J. Rose-Hansen, for interest, assistance and organizational help. We appreciate the professional help of Mr. Ng Sinh, Mrs. Berit Wenzell, Mrs. Camilla Sarantaris and Mrs. Britta Munch as well as the valuable

TABLE 3. NERNST PARTITION COEFFICIENTS MELT–ALLOY AND *mss*–ALLOY FOR SELECTED EXPERIMENTAL RUNS

Run no.	Alloy composition*		Melt or <i>mss</i> composition			Os in melt or <i>mss</i> Os in alloy **
	Os	Fe	Os	Fe	S	
1180°C						
melt						
1	7.09	92.83	0.01	56.75	43.24	1.410×10^{-3}
2	16.2	83.74	0.01	57.05	42.93	6.173×10^{-4}
3	30.99	68.85	≤ 0.02	-	-	$< 6.454 \times 10^{-4}$
41	21.02	78.79	0.01	-	-	4.757×10^{-4}
41'	27.29	72.68	0.01	-	-	3.664×10^{-4}
42	37.96	31.92	0.01	-	-	2.634×10^{-4}
4	43.64	56.18	0.01	56.48	43.51	2.291×10^{-4}
5	55.63	43.99	0.01	53.7	46.3	1.798×10^{-4}
6	74.89	24.65	0.02	53.74	46.24	2.671×10^{-4}
7	96.42	3.19	0.03	50.41	49.56	3.112×10^{-4}
<i>mss</i>						
38	81.27***	18.36	0.12	50.6	49.28	1.477×10^{-3}
39	90.18***	9.71	0.09	50.09	49.82	9.980×10^{-4}
40	89.43***	10.39	0.06	50.03	49.91	6.709×10^{-4}
8	99.16	0.6	0.37	47.19	52.44	3.731×10^{-3}
11'	99.66	0.17	0.62	46.61	52.76	6.221×10^{-3}
14'	99.55	0.18	0.46	47.23	52.31	4.621×10^{-3}
15'	99.8	0.05	0.57	46.83	52.6	5.711×10^{-3}
1100°C						
melt						
1	13.75	86.02	0.01	56.14	43.85	7.273×10^{-4}
2	26.12	73.69	0.01	55.35	44.65	3.828×10^{-4}
41	27.29	72.68	0.01	-	-	3.664×10^{-4}
41'	20.19	79.66	0.01	-	-	4.953×10^{-4}
3	33.43	66.35	0.01	53.53	46.42	2.991×10^{-4}
4	41.74	58.01	0.01	54.07	45.92	2.396×10^{-4}
5	50.81	48.72	0.01	53.85	46.14	1.968×10^{-4}
6	63.32	36.25	0.02	52.75	47.23	3.159×10^{-4}
<i>mss</i>						
7	74.19***	25.42	0.04	49.97	49.99	5.392×10^{-4}
7'	97.88	1.64	0.04	49.97	49.99	4.087×10^{-4}
8	98.86	0.85	0.12	48.84	51.03	1.214×10^{-3}
9'	98.76 ***	0.78	0.43	46.38	53.19	4.354×10^{-3}
11'	99.29	0.1	0.45	46.92	52.63	4.532×10^{-3}
13'	99.09	0.43	0.34	46.96	52.7	3.431×10^{-3}
900°C						
<i>mss</i>						
10	6.49	93.42	0.02	49.93	50.06	3.082×10^{-3}
11	14.37	85.54	0.01	49.92	50.08	6.959×10^{-4}
12	25.91	73.96	0.01	49.85	50.14	3.860×10^{-4}
1	32.44	67.39	0.02	50.39	49.59	6.165×10^{-4}
13	41.19	58.65	0.02	49.72	50.26	4.855×10^{-4}
14	48.97	50.93	0.05	49.65	50.3	1.021×10^{-3}
2	81.04***	18.57	0.11	50.04	49.85	1.357×10^{-3}
2'	56.36***	43.35	0.11	50.04	49.85	1.952×10^{-3}
3	57.08***	42.68	0.07	49.58	50.35	1.226×10^{-3}
3'	98.86***	0.67	0.07	49.58	50.35	7.081×10^{-4}
15	60.54***	38.73	0.09	49.5	50.42	1.487×10^{-3}
16	82.68***	16.89	0.13	49.19	50.68	1.572×10^{-3}
17	87.37***	12.21	0.09	49.48	50.43	1.030×10^{-3}
17'	96.61	3.25	0.09	49.48	50.43	0.932×10^{-4}
18	99.24	0.5	0.11	47.89	52	1.108×10^{-3}
4'	99.76	0.07	0.29	47.63	52.08	2.907×10^{-3}
5'	99.51	0.1	0.27	47.38	52.35	2.713×10^{-3}

Compositions are expressed in at.%. The ratio Os in melt or *mss* / Os in alloy is a ratio of atom proportions. * Spurious to minor S from correction errors or analyses on small grains. ** For all melt and *mss* compositions quoted with 0.01 at.% Os, the partition coefficient is smaller than or equal to the quoted value. *** Appreciable spread of alloy compositions in the charge. † three-phase runs containing alloy – melt or *mss* – OsS_2 .

comments of the referee, Dr. L.J. Cabri and of the editor-in-chief, Prof. R.F. Martin. This research was supported by the State Research Council (Natural Science) of Denmark, no. 940111.

REFERENCES

- AUGÉ, T. & LEGENDRE, O. (1992): Pt–Fe nuggets from alluvial deposits in eastern Madagascar. *Can. Mineral.* **30**, 983–1004.
- BOWLES, J.F.W., ATKIN, D., LAMBERT, J.L.M., DEANS, T. & PHILLIPS, R. (1983): The chemistry, reflectance, and cell size of the erlichmanite (OsS₂)–laurite (RuS₂) series. *Mineral. Mag.* **47**, 465–471.
- CABRI, L.J., ed. (1981): Platinum-Group Elements: Mineralogy, Geology, Recovery. *Can. Inst. Mining Metall., Spec. Vol.* **23**.
- _____, HARRIS, D.C. & WEISER, T.W. (1996): Mineralogy and distribution of platinum-group mineral (PGM) placer deposits of the world. *Explor. Mining Geol.* **5**, 73–167.
- FISHMAN, B.A., PAVLYUCHENKO, N.M., BLAGOVESHCHENSKAYA, N.V., BRYUKVIN, V.A., BLOKHINA, L.I. & BYALYI, A.V. (1992): A study of eutectic equilibrium in the Os–S and Ir–S systems. *Izv. Akad. Nauk SSSR, Metally* **1992**(4), 51–54 (in Russ.).
- JOHAN, Z., OHNENSTETTER, M., SLANSKY, E., BARRON, L.M. & SUPPEL, D. (1989): Platinum mineralization in the Alaskan-type intrusive complexes near Fifield, New South Wales, Australia. 1. Platinum-group minerals in clinopyroxenes of the Kelvin Grove Prospect, Owendale intrusion. *Mineral. Petrol.* **40**, 289–309.
- KARUP-MØLLER, S. & MAKOVICKY, E. (1999): The phase system Fe–Re–S at 1200°, 1100°, 1000°, and 900°C. *Neues Jahrb. Mineral., Monatsh.*, 265–280.
- KUBASCHEWSKI, O. (1982): *Iron – Binary Phase Diagrams*. Springer, New York, N.Y.
- MASSALSKI, T.B., MURRAY, J.L., BENNETT, L.H. & BAKER, H. (1986): *Binary Alloy Phase Diagrams* **1** and **2**. American Society for Metals, Metals Park, Ohio.
- PEARSON, D.I.C. & WILLIAMS, J.M. (1979): ⁵⁷Fe Mössbauer study of hexagonal phase iron alloys. *J. Phys. F: Metal Phys.* **9**, 1797–1813.
- SWARTENDRUBER, L.J. (1983): The Fe–Os (iron–osmium) system. *Bull. Alloy Phase Diagrams* **4**, 396–399.

Received July 30, 2000, revised manuscript accepted August 12, 2001.